Self-Assembly of Hierarchically Mesoporous–Macroporous Phosphated Nanocrystalline Aluminum (Oxyhydr)oxide Materials

ARTICLE *in* CHEMISTRY OF MATERIALS · MARCH 2006

Impact Factor: 8.35 · DOI: 10.1021/cm0520160

Self-Assembly of Hierarchically Mesoporous−Macroporous Phosphated Nanocrystalline Aluminum (Oxyhydr)oxide Materials

Zhong-Yong Yuan,[†,‡] Tie-Zhen Ren,[†] Ammar Azioune,[§] Jean-Jacques Pireaux,[§] and Bao-Lian Su*[,†]

Laboratoire de Chimie des Matériaux Inorganiques (CMI), and Laboratoire Interdisciplinaire de Spectroscopie Electronique (LISE), University of Namur (FUNDP), 61 rue de Bruxelles, B-5000 Namur, Belgium, and Department of Materials Chemistry, Nankai University, Tianjin 300071, People's Republic of China

Received September 7, 2005. Revised Manuscript Received February 1, 2006

A hierarchical structure of mesoporous−macroporous phosphated aluminum (oxyhydr)oxide (PAl) materials was prepared via a simple self-assembly process with the use of precursor aluminum *sec*-butoxide in a mixed solution of H_3PO_4 and Na_2HPO_4. Direct phosphation resulted in the incorporation of phosphorus into the inorganic framework of aluminum (oxyhydr)oxides by the Al−O−P bonds. The X-ray diffraction (XRD) patterns revealed that, despite slight phosphorus incorporation or phosphation, the frameworks of the as-synthesized autoclaved PAl samples remained in a crystalline phase of boehmite AlOOH-type, and their calcined products had a phase of γ-Al_2O_3-type. The macroporous structures are uniform, with sizes of 500−1800 nm, and the macropore walls are composed of accessible mesopores of a scaffold-like nanoparticle assembly. It is shown that the direct incorporation of phosphorus from a phosphate solution of the synthesis system can stabilize the framework of mesoporous−macroporous aluminum oxides with high surface areas and acidic properties. The present study also demonstrated that the surfactant (Brij 56) did not seem to have a direct role in the formation of macroporous structures, but significantly influenced the textural properties of the resultant PAl materials. The surface areas of surfactant-synthesized PAl exceeded 700 m^2/g, which is almost two times of that of surfactantless-synthesized samples. The synthesized hierarchical PAl exhibited high thermal stability (at least 800 °C), possessing surface hydroxyl groups and acid sites, which may attract much interest for practical applications, including catalysis.

Introduction

Activated aluminum oxides are technically important materials with a broad range of utilities not only in catalysis (as catalyst and catalyst support), but also adsorption and separation,[1] the performances of which are, to a great extent, basically relying on their surface area and porosity. Organized mesoporous aluminas are thus synthesized via the utilization of supramolecular templating methods in the presence of ionic or nonionic surfactants or co-polymers,[2] in view of the industrial demand of a narrow pore size distribution with a high surface area and large pore volume. However, the amorphous and semicrystalline nature of the prepared mesoporous aluminum oxides would limit their hydrothermal stability and greatly compromise their usefulness in catalytic applications,[3,4] because calcination at high temperature may cause the collapse of mesoporous framework and the loss of surface area, because of the facile crystallization of alumina and the subsequent crystal growth. It is still a challenge to synthesize mesoporous alumina with a controllable crystalline phase, high crystallinity, hierarchical porosity, and a large surface area.

In practical catalytic applications, doping with small amounts of foreign anions or cations is often empirically observed to improve the overall performance of the catalytic alumina and supposed to act as a crystal phase and/or surface area stabilizer.[5] Phosphates have been claimed to play the role of support stabilizers, and also to modify, in a potentially convenient way, some of the acid−base surface properties of the active carrier,[5−7] although the role of the phosphate species, either as a support stabilizer or as a chemical promoter, is still not totally known. It has been shown that, upon impregnation of γ-alumina with phosphoric acid, partial solubilization of the Al^{3+} cations occurs, leading to the precipitation of $AlPO_4$ during the drying procedure.[8] More-

* Author to whom correspondence should be addressed. Tel.: +32-81-72-4531. Fax: +32-81-725414. E-mail: bao-lian.su@fundp.ac.be.

† Laboratoire de Chimie des Matériaux Inorganiques (CMI), University of Namur (FUNDP).

§ Laboratoire Interdisciplinaire de Spectroscopie Electronique (LISE), University of Namur (FUNDP).

‡ Nankai University.

(1) Wefers, K.; Misra, C. Oxides and Hydroxides of Aluminum; Aloca Technical Paper 19, Alcoa Laboratories, Alcoa Center, PA, 1987.
(2) Čejka, J. *Appl. Catal., A* **2003**, *254*, 327−338, and the references therein.
(3) Hicks, R. W.; Pinnavaia, T. J. *Chem. Mater.* **2003**, *15*, 78−82.
(4) Zhang, Z.; Hicks, R. W.; Pauly, T. R.; Pinnavaia, T. J. *J. Am. Chem. Soc.* **2002**, *124*, 1592−1593.
(5) Mekhemer, G. A. H.; Nohman, A. K. H.; Fouad, N. E.; Khalaf, H. A. *Colloids Surf. A* **2000**, *161*, 439−446.
(6) Gishti, K.; Iannibello, A.; Marengo, S.; Morelli, G.; Tittarelli, P. *Appl. Catal.* **1984**, *12*, 381−393.
(7) Mennour, A.; Ecolivet, C.; Cornet, D.; Hemidy, J. F.; Lavalley, J. C.; Mariette, L.; Engelhard, P. *Mater. Chem. Phys.* **1988**, *19*, 301−313.
(8) López Cordero, R.; Gil Llambias, F. J.; Palacios, J. M.; Fierro, J. L. G.; López Agudo, A. *Appl. Catal.* **1989**, *56*, 197−206.

10.1021/cm0520160 CCC: $33.50
Published on Web 03/09/2006

over, the introduction of small amounts of PO_4^{3-} ions has been determined to enhance the surface acidity property of alumina remarkably,[5,9] leading to the improved catalytic activities of the resultant phosphated alumina catalysts in several acid-catalyzed reactions.

The conventional method to introduce the phosphoric ions is post-treatment (wet impregnation) with phosphate compounds, e.g., $(NH_4)_2HPO_4$, $(NH_4)H_2PO_4$, and H_3PO_4, in which H_3PO_4 has been observed to be an excellent candidate to improve the thermal stability and acidity of mesoporous materials greatly.[10−12] The P−OH bond in H_3PO_4 can react with the uncondensed surface hydroxyl groups of the mesoporous materials, leading to complete cross-linking. Furthermore, H_3PO_4 can be polymerized to polyphosphoric acid with a network structure at high temperatures. This network structure, which is tightly attached to the surface of mesoporous materials, can effectively resist the shrinkage of pore channels during thermal or hydrothermal treatment.[11] However, to the best of our knowledge, there is no report on the synthesis of phosphated mesoporous aluminum (oxyhydr)oxides by directly incorporating phosphorus from phosphate compounds in the synthesis systems of mesoporous materials.

Recent interest is being devoted to the development of hierarchically ordered porous structures at multiple length scales,[13,14] because hierarchical materials with different pore sizes integrated in one body can be expected to combine reduced resistance to diffusion and high surface areas for yielding improved overall reaction and adsorption/separation performances and can be extended to biological applications. Very recently, bimodal macroporous−mesoporous aluminum oxide materials[15,16] have been prepared in the presence of one single surfactant without needing the secondary templates such as colloid crystals[17,18] or emulsion/vesicle droplets[19,20] for the formation of macropores. Microwave heating was also used to produce hierarchically mesoporous−macroporous crystalline aluminum (oxyhydr)oxides of good quality with high surface areas and large pore volumes.[16] The synthesized aluminum (oxyhydr)oxide particles have parallel arrays of channel-like macropores that are interconnected with mesopores, which are of considerable interest for their potential applications in catalysis and separation processes, because of the enhanced access to the mesopores, as provided by the regularly arrayed macropores. Initial work suggested that the single surfactant would direct the formation of inorganic phases with multidimensional pore systems.[15,16,21] However, other experiments revealed that the similar macroporous structures could be spontaneously formed in the absence of a surfactant.[22−25] Although the formation mechanism of such hierarchical macroporous structures is not totally understood, their practical applications in catalysis have been emerging.[26]

Thus, it is significant to develop one facile and effective method to synthesize phosphated aluminum oxide-based materials with controlled multiscale porosity. Herein, we report the self-formation of phosphated nanocrystalline aluminum (oxyhydr)oxide materials with a uniform macroporous system with mesoporous walls. The effects of phosphates on mesoporous−macroporous aluminum oxides, from the point of view of the structural, morphological, and surface chemical features, and the influence of the surfactant on the formation of the hierarchical porous structures were examined.

Experimental Section

Preparation. All chemicals were used as received, without further purification. In a typical synthesis procedure for phosphated aluminum (oxyhydr)oxides (designated as PAl), 6 or 12 mL of Na_2HPO_4 solution (0.1 mol/L) was mixed in 55 mL of a H_3PO_4 aqueous solution (pH 2) to form a buffer solution in the presence or absence of 6.67 g (0.01 mol) surfactant Brij 56 ($C_{16}H_{33}(OCH_2CH_2)_nOH$, $n \approx 10$, Aldrich) at 40 °C under stirring, followed by the addition of aluminum *sec*-butoxide (Fluka, 5.0 g) with phosphate/aluminum molar ratio of 1:2 or 2:2 (the resulted samples were denoted as P_1Al_2 or P_2Al_2, respectively). A buffer solution is used to stabilize the pH value and avoid a sudden change in pH value that would be due to the hydrolysis and polycondensation during the entire synthesis procedure. After a further stirring of 2 h at room temperature, the obtained mixture was separated into two parts: one was transferred into a Teflon-lined autoclave and heated statically in an oven at 80 °C for 24 h, and another was directly filtered, washed with water, and dried at 60 °C for comparison. The autoclaved products were then calcined at 500 °C for 4 h to remove the occupied organic species and further calcined at 650 or 800 °C for 1 h to investigate their thermal stabilities. The resultant samples were denoted as PAl-d and PAl-h for the as-synthesized nonautoclaved and autoclaved products, respectively, and PAl-c500, PAl-c650, and PAl-c800 for the calcined products of PAl-h at 500, 650, and 800 °C, respectively.

Characterization. Powder X-ray diffraction (XRD) patterns were recorded on a Philips PW1820 diffractometer with Cu Kα radiation. N_2 adsorption and desorption isotherms were obtained on a Micromeritics Tristar 3000 system at liquid nitrogen temperature. The samples were degassed at 80 °C overnight before measurements were made. The specific surface area was determined by the Brunauer−Emmett−Teller (BET) method, and the mesopore size

(9) Abbattista, F.; Delastro, A.; Gozzelino, G.; Mazza, D.; Vallino, M.; Busca, G.; Lorenzelli, V. *J. Chem. Soc., Faraday Trans.* **1990**, *86*, 3653−3658.
(10) Kolonia, K. M.; Petrakis, D. E.; Ladavos, A. K. *Phys. Chem. Chem. Phys.* **2003**, *5*, 217−222.
(11) Huang, L. M.; Li, Q. Z. *Chem. Lett.* **1999**, *28*, 829−830.
(12) Yu, J. C.; Zhang, L.; Zheng, Z.; Zhao, J. *Chem. Mater.* **2003**, *15*, 2280−2286.
(13) Soten, I.; Ozin, G. A. *Curr. Opin. Colloid Interface Sci.* **1999**, *4*, 325−337.
(14) Su, B. L.; Léonard, A.; Yuan, Z. Y. *C. R. Chim.* **2005**, *8*, 713−726.
(15) Deng, W. H.; Toepke, M. W.; Shanks, B. H. *Adv. Funct. Mater.* **2003**, *13*, 61−65.
(16) Ren, T. Z.; Yuan, Z. Y.; Su, B. L. *Langmuir* **2004**, *20*, 1531−1534.
(17) Holland, B. T.; Blanford, C. F.; Do, T.; Stein, A. *Chem. Mater.* **1999**, *11*, 795−805.
(18) Lebeau, B.; Fowler, C. E.; Mann, S.; Farcet, C.; Charleux, B.; Sanchez, C. *J. Mater. Chem.* **2000**, *10*, 2105−2108.
(19) Antonelli, D. M. *Microporous Mesoporous Mater.* **1999**, *33*, 209−214.
(20) Yuan, Z. Y.; Ren, T. Z.; Su, B. L. *Adv. Mater.* **2003**, *15*, 1462−1465.
(21) Blin, J. L.; Léonard, A.; Yuan, Z. Y.; Gigot, L.; Vantomme, A.; Cheetham, A. K.; Su, B. L. *Angew. Chem., Int. Ed.* **2003**, *42*, 2872−2875.
(22) Ren, T. Z.; Yuan, Z. Y.; Su, B. L. *Chem. Commun.* **2004**, 2730−2731.
(23) Léonard, A.; Su, B. L. *Chem. Commun.* **2004**, 1674−1675.
(24) Collins, A.; Carriazo, D.; Davis, S. A.; Mann, S. *Chem. Commun.* **2004**, 568−569.
(25) Deng, W.; Shanks, B. H. *Chem. Mater.* **2005**, *17*, 3092−3100.
(26) Wang, X.; Yu, J. C.; Ho, C.; Hou, Y.; Fu, X. *Langmuir* **2005**, *21*, 2552−2559.

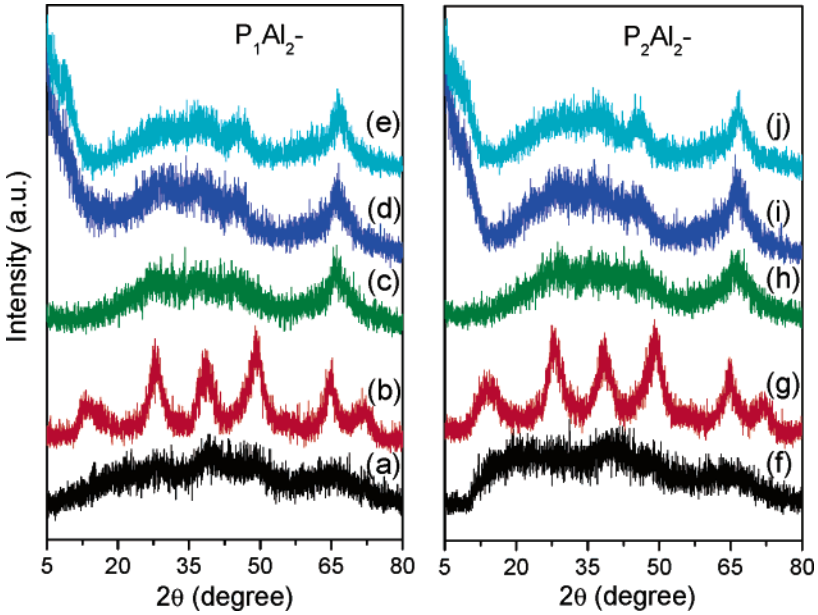

Figure 1. Wide-angle X-ray diffraction (XRD) patterns of the PAl samples synthesized in the absence of Brij 56: (a) P_1Al_2-d, (b) P_1Al_2-h, (c) P_1Al_2-c500, (d) P_1Al_2-c650, (e) P_1Al_2-c800, (f) P_2Al_2-d, (g) P_2Al_2-h, (h) P_2Al_2-c500, (i) P_2Al_2-c650, and (j) P_2Al_2-c800.

distribution was obtained from the N_2 adsorption branch of isotherms, using the Barrett−Joyner−Halenda (BJH) method, as commonly suggested.[14,16]

Scanning electron microscopy (SEM) and transmission electron microscopy (TEM) analyses were conducted with a Philips XL-20 system at 15 keV and a Philips TECNAI-10 system at 100 kV, respectively. The specimens for TEM observation were prepared using epoxy-resin-imbedded microsectioning and mounting on a copper grid. Thermogravimetry (TG) analysis was performed in a dry flowing air on a SETARAM TG-DSC 111 thermoanalyzer at a heating rate of 1 °C/min using alumina as the reference.

Solid-state ^{27}Al and ^{31}P magic angle spinning (MAS) nuclear magnetic resonance (NMR) spectra were recorded on a Bruker model MSL-400 spectrometer operating at resonance frequencies of 104.3 and 161.9 MHz, and 1.0 μs ($\theta = \pi/12$) and 2.5 μs ($\theta = \pi/6$) pulses with repetition times of 0.2 and 10 s, respectively. Chemical shifts were referenced to $[Al(H_2O)_6]^{3+}$ for ^{27}Al and to H_3PO_4 (85%) for ^{31}P.

X-ray photoelectron spectroscopy (XPS) measurements were realized on a Hewlett−Packard model 5950A spectrometer that was equipped with a monochromatic Al Kα source (1486.6 eV). Charging effects were neutralized using a flood gun typically operated at 2 eV. The take-off angle analysis, relative to the surface, was 52°. All the spectra showed a small shift due to charging and were therefore calibrated in relation to the C_{1s} peak of contamination (285.0 eV). The photoemission peaks were fitted with mixed Gaussian−Lorentzian functions using a home-developed (LISE) least-squares curve-fitting program (Winspec). Both linear and Shirley backgrounds were used, depending on the shape of spectra. The surface atomic composition was calculated by the integration of the peak areas on the basis of the Scofield's sensitivity factors.

Fourier transform infrared (FT-IR) spectroscopy was performed with a Perkin−Elmer Spectrum 2000 spectrometer. The KBr pellet technique was used for the framework vibration characterization. For the study of the surface acidity, a self-supported wafer of sample (10−20 mg) was evacuated in situ (10^{-5} Torr) at 450 °C for 3 h, followed by adsorption of NH_3 at room temperature for 15 min, and desorption at different temperatures (100−300 °C) for 15 min, respectively.

Results and Discussion

X-ray Diffraction. Both the wide-angle and low-angle powder XRD patterns were measured to determine the crystal and structural phases of the as-synthesized and calcined PAl samples. Figure 1 shows the wide-angle XRD patterns of the PAl samples synthesized in the absence of a surfactant. The samples synthesized in the presence of a surfactant presented similar patterns. The nonautoclaved samples P_1Al_2-d and P_2Al_2-d are almost amorphous, although their diffractions seem to be similar to that of the boehmite phase. The autoclaved samples P_1Al_2-h and P_2Al_2-h exhibited good diffraction lines that were assignable to the boehmite phase AlOOH (JCPDS Card No. 21-1307), which was consistent with the surfactant-directed (macroporous−)mesoporous materials resulting from the assembly of AlOOH nanoparticles.[3,16] The weak and broad diffraction peaks indicate that the samples were composed of small crystals with a nanometer-scale crystalline size and/or relatively low crystallinity, and the calculation by the Scherrer equation, despite its accuracy, revealed crystalline grain sizes of 1.8−2.1 nm. After calcination at 500 °C, the boehmite structure disappeared and one broadened diffractogram was presented that could correspond to the γ-structure of alumina (Al_2O_3) (see panels c and h of Figure 1). Furthermore, calcination at higher temperature, even 800 °C, did not cause the higher degree of crystallization of the resultant PAl samples (see panels e and j of Figure 1), and no detectable $AlPO_4$ bulk phase was found in all cases. It is reported that the γ-Al_2O_3 phase is formed upon the dehydration of the aluminum oxyhydroxide boehmite at temperatures in the range of 400−700 °C.[27] Moreover, the diffraction peaks of our previous reported mesoporous−macroporous γ-Al_2O_3 (the calcined product of mesoporous−macroporous boehmite AlOOH at 400−500 °C)[16] are quite stronger than those of the present

(27) Misra, C. *Industrial Alumina Chemicals*; ACS Monograph 184; American Chemical Society: Washington, DC, 1986.

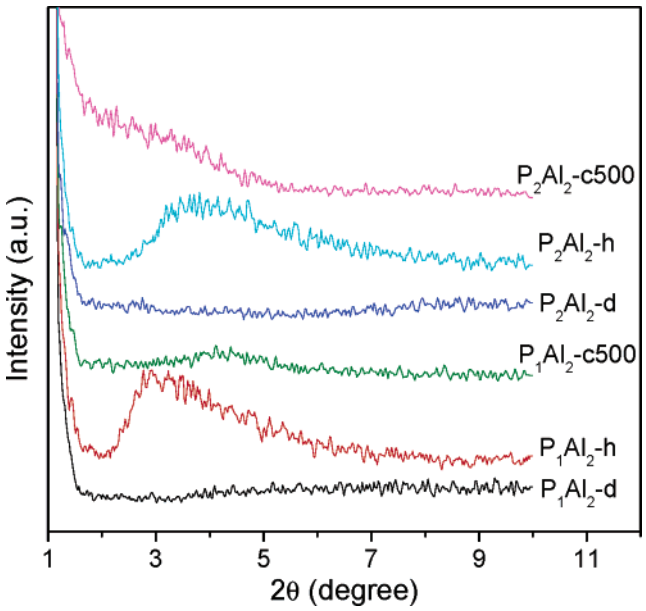

Figure 2. Low-angle XRD patterns of the PAl samples synthesized in the presence of surfactant Brij 56.

PAl samples that were calcined at 500−800 °C. This may suggest that the phosphation of alumina prevents nanocrystal growth during high-temperature calcination.

Surfactant-templated mesoporous materials are normally supposed to show one or more diffraction peaks at low-angle range. Thus, the low-angle XRD patterns of the PAl samples synthesized in the presence of surfactant Brij 56 were measured, and the results are presented in Figure 2. The nonautoclaved samples PAl-d, regardless of the P/Al ratios in their synthesis gel, did not exhibit any low-angle diffraction peaks in the 2θ range of 1°−10°, whereas the autoclaved samples PAl-h displayed one broad peak in the 2θ range of 2°−5°. Such very broad diffractions were also observed in the autoclaved and 500 °C-calcined samples PAl-c500, but with very low intensity. These low-angle diffractions may result more from the packing of regularly sized alumina nanoparticles than from the so-called surfactant-templated mesostructures.[28] No narrow peaks in the 2θ range of 1°−3°, that is characteristic of an ordered mesostructure, were observed in the synthesized PAl samples; therefore, it is believed that there is no long-range order of mesopores in these PAl materials, although we cannot exclude the possibility of the peaks at a 2θ angle of <1.3°, because of the limit of our diffractometer. Nevertheless, in regard to the PAl samples synthesized in the absence of a surfactant, no low-angle diffractions were observed in all samples.

Nitrogen Adsorption Analysis. The nitrogen adsorption−desorption isotherms, and the corresponding pore size distributions, of the PAl samples synthesized in the presence and absence of a surfactant are shown in Figures 3 and 4 and in the Supporting Information; their textural properties are listed in Table 1. An identical evolution was revealed as a function of different treatment for both the P_1Al_2 and P_2Al_2 series. The isotherms of the PAl-d samples synthesized in the presence of a surfactant are of classical type IV with a hysteresis loop of type H2 (Figure 3), which is indicative of mesoporosity, good pore connectivity, and the presence of pores with narrow mouths (ink-bottle pores).[29] Also, one single narrow peak centered at 4.1−4.5 nm was observed in their corresponding pore size distribution curves (determined by the BJH method from the adsorption branch of the isotherms). This porosity should be as a result of the organized aggregation of alumina nanoparticles that was the hydrolysis product of aluminum alkoxide. It is noted that the isotherms of these PAl-d samples presented a strong uptake at very high relative pressure ($P/P_0 > 0.9$), which could suggest an appreciable amount of secondary porosity of very large pores (macropores). Nevertheless, their BET surface areas are relative low (189 m^2/g for P_1Al_2-d and 223 m^2/g for P_2Al_2-d).

However, the surfactant-synthesized PAl-h samples show adsorption−desorption isotherms that have a very strong increase of nitrogen-adsorbed volume at P/P_0 higher than 0.85, and their corresponding pore size distributions present one broad peak in the range of 5−45 nm, besides one narrow peak at ∼3 nm. Moreover, very high surface areas and large pore volumes are obtained (732 m^2/g and 3.4 cm^3/g for P_1Al_2-h, and 643 m^2/g and 2.7 cm^3/g for P_2Al_2-h, respectively). This is really different with the pure AlOOH mesoporous−macroporous structures synthesized with the same surfactant,[16] indicating the effect of phosphation on the structural and textural properties of the hierarchical aluminum oxides. Calcination of these PAl-h samples leads to a decrease in their surface areas and the broadening of their pore size distributions (Table 1), and the surface areas decrease and pore size distributions broaden with the increase of the calcination temperature. Interestingly, very high surface areas (>359 m^2/g) can still be obtained after calcination at 800 °C, indicating the high thermal stability of these surfactant-synthesized PAl samples. It is particularly noteworthy that the present phosphated aluminum oxide samples (PAl-h and PAl-c500) have surface areas (495−732 m^2/g) substantially larger than those of the previously reported mesoporous−macroporous pure aluminum oxide (boehmite and γ-alumina, 380−435 m^2/g).[16]

The isotherms of the PAl samples synthesized in the absence of a surfactant, regardless of whether the synthesis occurred before and after calcination, are all type IV with a hysteresis loop of H2 type (Figure 4), which are similar with surfactant-synthesized PAl-d, and previously reported pure crystalline mesoporous−macroporous aluminum oxides.[16] The PAl-h samples show narrower pore size distributions (centered 2.4−2.7 nm) than the PAl-d samples (4.3−5.0 nm). After calcination at 500 °C, the pore sizes of PAl-h were enlarged to 3.6−3.7 nm, which were further enlarged with increasing calcination temperature, accompanying the broadening of the pore size distributions. The BET surface areas of PAl-h are higher than those of PAl-d, and decrease with the increase of calcination temperature, as similar as the case of the surfactant-synthesized PAl samples. However, the surface areas of these nonsurfactant-synthesized PAl-h and

(28) Vantomme, A.; Yuan, Z. Y.; Su, B. L. *New J. Chem.* **2004**, *28*, 1083−1085.

(29) Gregg, S. J.; Sing, K. S. W. *Adsorption, Surface Area and Porosity*; Academic Press: London, 1997; pp 111−194.

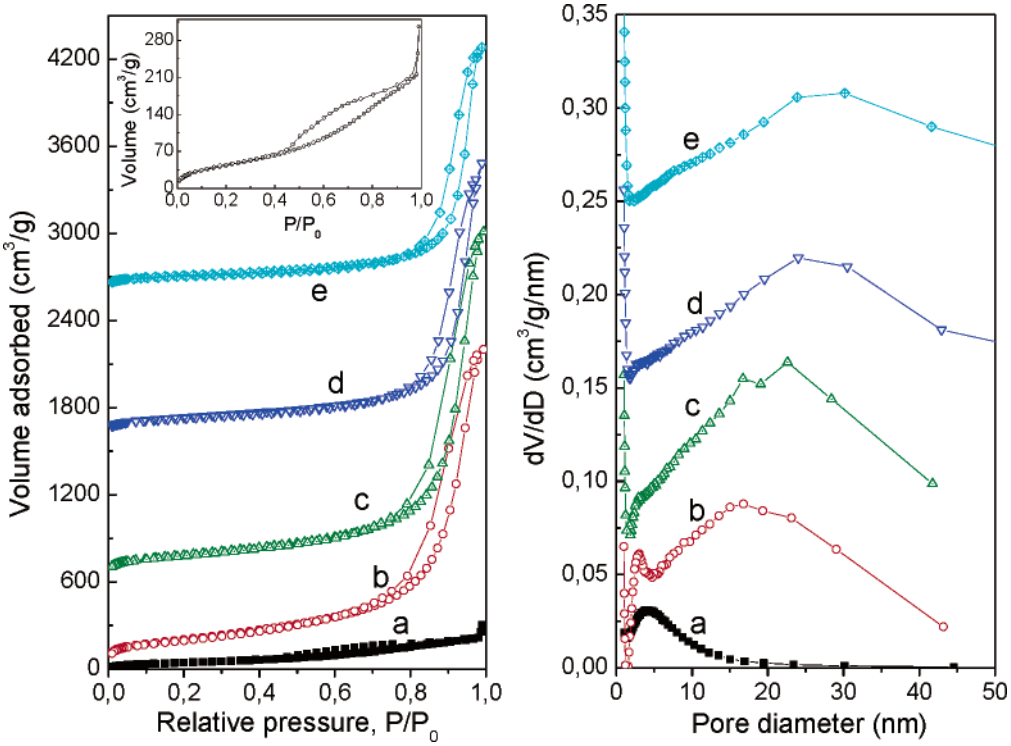

Figure 3. (left) N_2 adsorption−desorption isotherms and (right) the corresponding pore size distribution curves of the P_1Al_2 samples synthesized in the presence of Brij 56: (a) P_1Al_2-d, (b) P_1Al_2-h, (c) P_1Al_2-c500, (d) P_1Al_2-c650, and (e) P_1Al_2-c800. Inset is the re-scaled adsorption−desorption isotherms of the plots for data set a. The volume adsorbed was shifted by 600, 1600, 2600 and the d*V*/d*D* value was shifted by 0.065, 0.15, and 0.25 for the curves of data sets c−e, respectively.

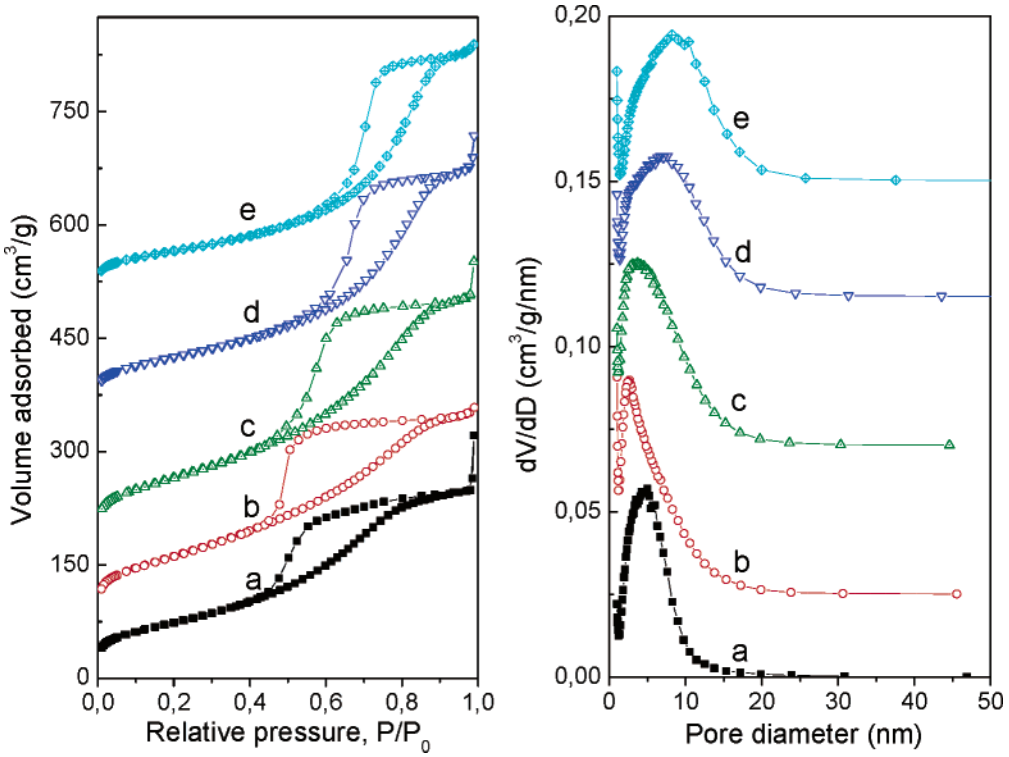

Figure 4. (left) N_2 adsorption−desorption isotherms and (right) the corresponding pore size distribution curves of the P_1Al_2 samples synthesized in the absence of Brij 56: (a) P_1Al_2-d, (b) P_1Al_2-h, (c) P_1Al_2-c500, (d) P_1Al_2-c650, and (e) P_1Al_2-c800. The volume adsorbed was shifted by 60, 170, 350, and 500 and the d*V*/d*D* value was shifted by 0.025, 0.07, 0.115, 0.15 for the curves of data sets b−e, respectively.

their calcination products are lower than those of surfactant-synthesized PAl samples, although the surface areas of PAl-d are slight higher than those of surfactant-synthesized samples, probably because of the surfactant occupation in the surfaces of surfactant-synthesized PAl-d. High surface areas of >200 m^2/g can still be seen in the nonsurfactant-synthesized PAl-c800 samples. This indicates that the autoclaving synthesis with a surfactant could efficiently result in the improvement of surface areas and pore volumes of the resultant PAl samples, as well as their thermal stability.

Table 1. Textural Properties of the Synthesized PAl Samples

sample	BET surface area, S_{BET} (m^2/g)	nitrogen pore volume, V_{pore}[a] (cm^3/g)	$D_{BJH-ads}$[b] (nm)	Average Pore Diameter, from BJH Analysis (nm)	
				adsorption, D_{av-ads}[c]	desorption, D_{av-des}[c]
Synthesized without Surfactant					
P_1Al_2-d	270	0.50	4.3	4.4	3.9
P_1Al_2-h	367	0.46	2.7	4.0	3.6
P_1Al_2-c500	349	0.59	3.7	4.7	4.2
P_1Al_2-c650	273	0.57	7.1	6.8	5.8
P_1Al_2-c800	235	0.52	8.2	7.3	6.4
P_2Al_2-d	276	0.44	5.0	4.9	4.3
P_2Al_2-h	377	0.44	2.4	3.7	3.5
P_2Al_2-c500	361	0.58	3.6	4.4	4.0
P_2Al_2-c650	265	0.49	6.7	6.1	5.2
P_2Al_2-c800	207	0.47	9.0	7.6	6.1
Synthesized with Surfactant					
P_1Al_2-d	189	0.47	4.1	5.3	4.3
P_1Al_2-h	732	3.41	3.0, 16.8	14.5	8.3
P_1Al_2-c500	659	3.73	22.6	17.0	9.1
P_1Al_2-c650	473	2.91	24.0	20.5	18.6
P_1Al_2-c800	392	2.60	30.1	22.7	19.9
P_2Al_2-d	223	0.55	4.5	5.3	4.4
P_2Al_2-h	643	2.65	2.9, 19.4	13.2	8.1
P_2Al_2-c500	495	2.61	23.0	16.1	9.2
P_2Al_2-c650	375	2.30	24.5	20.8	17.9
P_2Al_2-c800	360	2.37	30.2	22.6	19.4
Al-h[d]	381	0.68	3.0	5.5	5.5
Al-c500[d]	424	1.01	8.8	7.3	6.3
Al-c650[d]	285	0.78	11.2	8.6	7.6
Al-c800[d]	234	0.75	12.2	9.9	8.4

[a] At $P/P_0 = 0.993$. [b] Maximum of BJH pore diameter distribution as determined from the adsorption branch. [c] BJH average pore diameter (4V/A). [d] Pure aluminum oxide has been reported in ref 16; as-synthesized Al-h is boehmite, and 500 °C-calcined Al-c500 is γ-alumina.

Scanning and Transmission Electron Microscopy. Figure 5 shows the representative scanning electron microscopy (SEM) images of the PAl samples synthesized with or without surfactant, revealing a uniform macroporous structure in all the samples, autoclaved or nonautoclaved, synthesized with or without surfactant, before or after calcination. The macropores are channel-like with sizes in the range of 500−1800 nm. The macrochannels are mainly of one-dimensional orientation, parallel to each other, perforative through almost the entire particle, which could be clearly seen from the side view of the samples (panels c and d of Figure 5). This is consistent with those observed in mesoporous−macroporous boehmite AlOOH and γ-Al_2O_3 synthesized in the presence of a surfactant.[16] Moreover, careful examination of these SEM micrographs reveals that the walls of the macropores are composed of small interconnected PAl granular particles. The fine particulate morphology indicates that the mesoporosity is probably partially due to the intraparticle porosity and partially due to the interparticle porosity.[26] Because no long-range ordered mesostructures are revealed by XRD, the mesoporosity observed from N_2 adsorption analysis is mainly due to the interparticle porosity.

The channel-like macroporous structures can be mostly preserved after calcination at elevated temperatures (500−800 °C). The surfaces of the sample particles became smoother after calcination (see panels f and g of Figure 5), bceause of the sintering and solidification of the macroporous framework and the boehmite-to-γ-alumina phase transition during the high-temperature treatment. Furthermore, there is almost no evident shrinkage of macropore sizes observed in the calcined PAl samples.

The well-defined macroporous structures were further confirmed using the TEM images of the microtomed specimens. Figure 6 shows the TEM images of surfactant-synthesized P_1Al_2-d, P_1Al_2-h, and P_1Al_2-c500 samples, being taken as representative. The wall thickness between the macropores with circular openings is ∼400−1000 nm. High-magnification TEM images make it obvious that the macropore walls of the nonautoclaved PAl-d specimens have a disordered wormhole-like mesopore structure formed by the agglomeration of granular nanoparticles, lacking discernible long-range order in the pore arrangement among the nanoparticles (see Figure 6c). Although the macroporous frameworks of both the autoclaved PAl-h and its calcination products are all composed of sheetlike or fibrous nanoparticles of PAl with a scaffold-like array of hierarchical ordering, and the scaffold-like aggregation and intergrowth of the nanofibers/nanosheets create the accessible mesoporous structures (see panels f and i of Figure 6), which are in agreement with those of the reported mesoporous−macroporous pure boehmite AlOOH and γ-alumina.[16] This difference in the macroporous frameworks is consistent with the crystalline phases observed in the XRD patterns (PAl-d is amorphous, and PAl-h and PAl-c are crystalline). It is also indicated that the topochemical transformation of macro-structured−mesostructured boehmite to γ-alumina did not result in the macro-mesostructural change upon such high-temperature treatment, as revealed by the retainability of the scaffold-like mesostructure and well-defined macroporous structure in the calcined products of PAl-h.

X-ray Photoelectron Spectroscopy. The surface stoichiometry characterization was performed by XPS. Figure 7

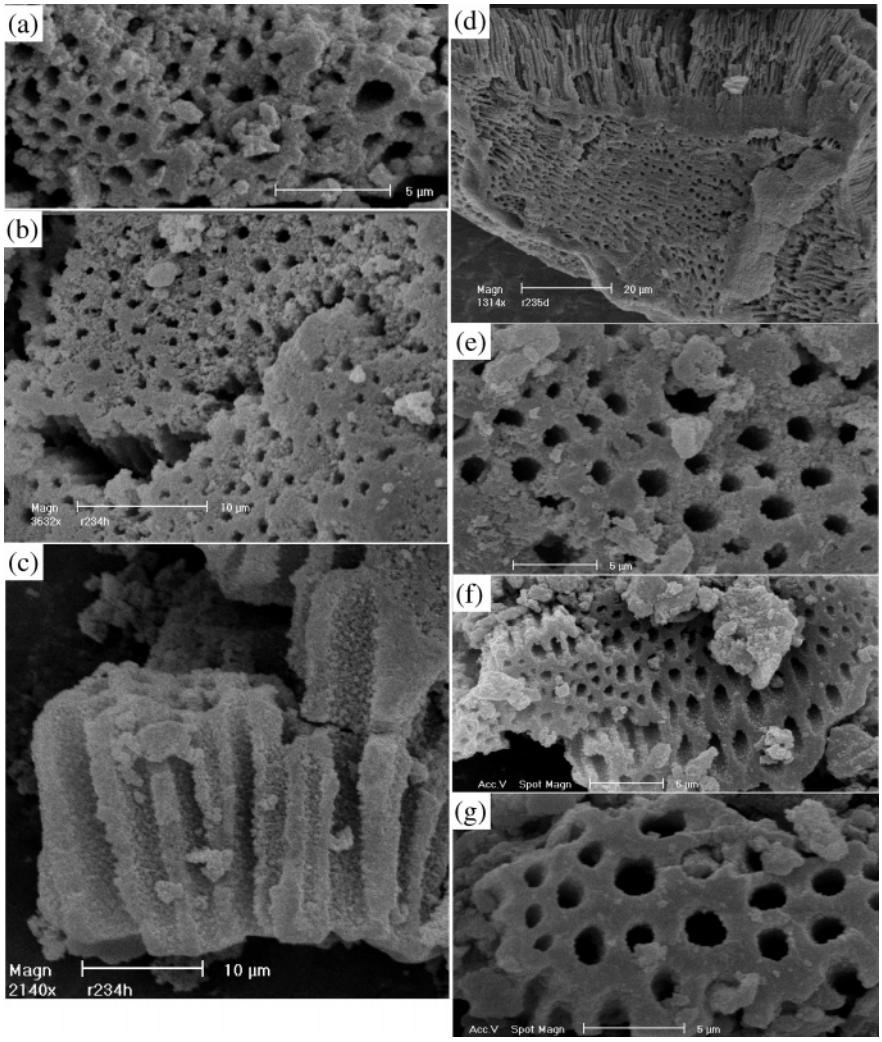

Figure 5. Scanning electron microscopy (SEM) images of the PAl samples synthesized in the presence of Brij 56 ((a) P_1Al_2-d, (b, c) P_1Al_2-h, (d) P_2Al_2-d, and (e) P_2Al_2-h), and the samples synthesized in the absence of Brij56 ((f) P_1Al_2-c500 and (g) P_2Al_2-c500).

shows the high-resolution XPS spectra of Al 2p, P 2p, and O 1s, taken on the surface of the P_1Al_2-h and P_1Al_2-c500 samples synthesized in the presence of a surfactant, which is taken as being representative. The binding energy of Al 2p and O 1s is ∼74.3 eV and ∼531.8 eV, respectively, corresponding to characteristic regions of aluminum oxide.[30] The P 2p binding energy of P_1Al_2-h is observed at 133.6 eV, which is characteristic of P^{5+},[31,32] and this signal shifts to 134.1 eV after 500 °C calcination of the sample. The broad O 1s line might be fitted by three components, situated at the binding energies of 530.8 ± 0.1, 532.1 ± 0.1, and 533.6 ± 0.1 eV with contributions of 35%, 52%, and 13% for P_1Al_2-h, and 49%, 37%, and 14% for P_1Al_2-c500, respectively. The peaks at 530.8 and 533.6 eV may correspond to oxygen combined with aluminum and carbon, respectively,[30] and main component of 532.1 eV may be the co-contribution of P−O bands and hydroxyl groups. The quantity of Al−O increased after calcination, and the total quantity of P−O and OH decreased, which is the result of dehydration during heat treatment. The surface atomic compositions of the PAl samples are summarized in Table 2. Only a small change is observed in the surface atomic compositions of the synthesized samples before and after calcination, in which the measured carbon component and the excess oxygen are from the surface-absorbed organic contaminant and the surface absorbed water, respectively. The Al/P ratios of the PAl samples are in the range of 8−13, regardless of whether the P/Al molar ratio of the initial gel was 1:2 or 2:2, which indicates stable phosphation by a similar quantity of phosphorus. This may be the effect of a buffer solution. Except for the surfactantless-synthesized P_1Al_2 sample, the Al/P ratios of the PAl-h and PAl-c500 samples are higher than that of PAl-d.

Solid-State NMR Spectroscopy. The local structure and environments in these samples were investigated by the solid-state MAS NMR technique, and the resultant ^{27}Al and ^{31}P MAS NMR spectra are shown in Figures 8 and 9, respectively. Data concerning the spectra are summarized in Table 2. In regard to the P_1Al_2 samples synthesized in the presence of a surfactant, the ^{27}Al NMR spectrum of a nonautoclaved P_1Al_2-d sample shows one broad peak at ∼7 ppm, whereas the autoclaved P_1Al_2-h gives one strong peak at 7 ppm, with two shoulder peaks at 0 and −14 ppm, and

(30) Fundamental XPS Data from Pure Elements, Pure Oxides, and Chemical Compounds, http://www.xpsdata.com/fundxps.pdf.
(31) Moulder, J. F.; Stickle, P. E.; Sobol, P. E.; Bomben, K. D. *Handbook of X-ray Photoelectron Spectroscopy*; Perkin−Elmer: Eden Prairie, MN, 1992.

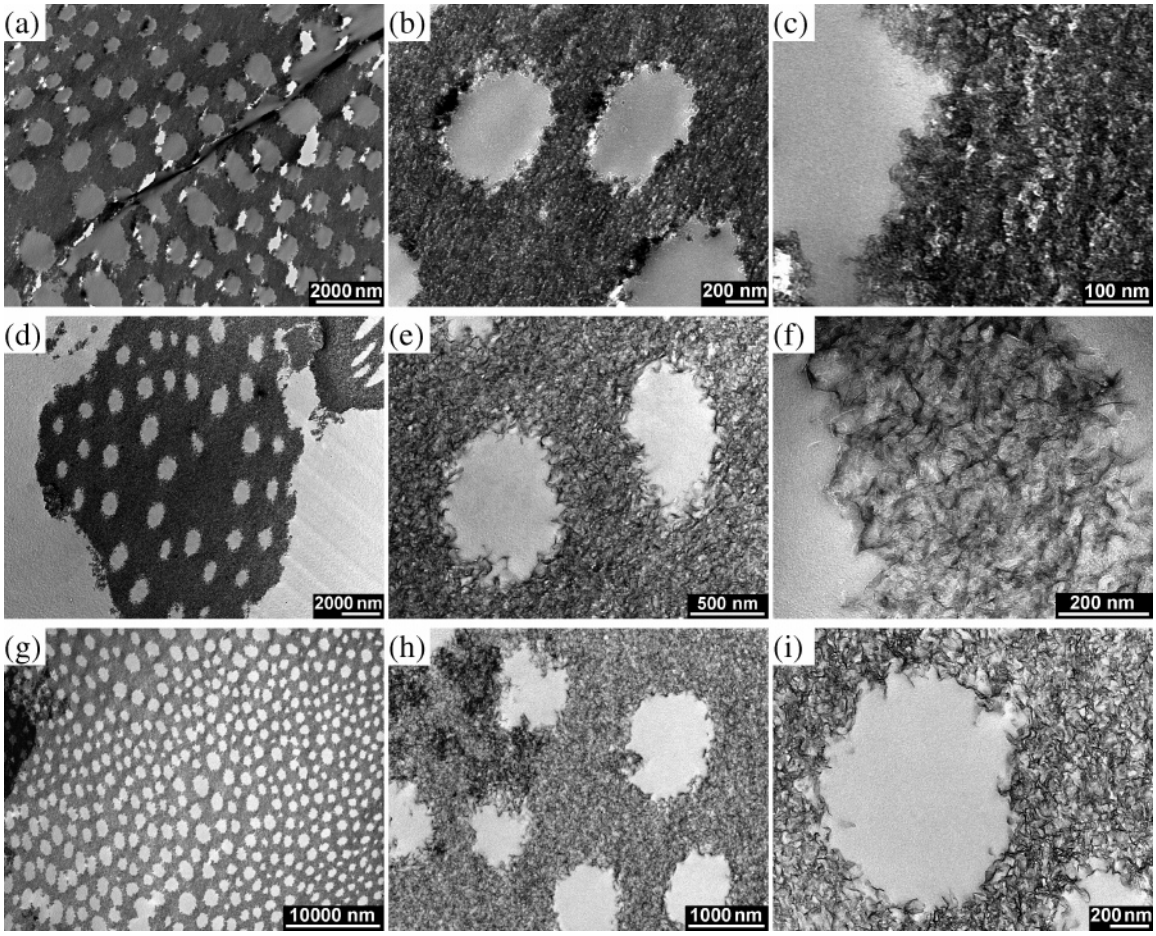

Figure 6. Cross-sectional transmission electron microscopy (TEM) images of the PAl samples synthesized in the presence of Brij 56, presented in different magnifications: (a, b, c) P_1Al_2-d, (d, e, f) P_1Al_2-h, and (g, h, i) P_1Al_2-c500.

its 500 °C-calcined product P_1Al_2-c500 presents one broad peak at ~67 ppm and one very weak peak at ~33 ppm, besides the main peak at 6 ppm (see Figure 8). The main peak of 6−7 ppm can be assigned to a six-coordinated Al species, and the broad peak at 67 ppm is attributed to four-coordinated Al, which are similar to the spectra of pure mesoporous−macroporous boehmite and γ-alumina.[16,33] The weak peak of 33 ppm is normally attributed to five-coordinated Al,[33] although signals in the range of 35−48 ppm were reported as characteristic of tetrahedral aluminum surrounded by four PO_4 groups in microporous $AlPO_4$ materials.[34,35] The shoulder peaks of 0 and −14 ppm can be assigned to octahedral species with water and phosphate ions in different environments.[35,36] Previous work has shown that the chemical shift of six-coordinated Al changes almost linearly with the number of phosphate groups in its coordinated shell, starting from 0 for $Al(H_2O)_6^{3+}$ and reaching −18 ppm for aluminum metaphosphate, where aluminum is coordinated to six PO_4 groups.[37] Rocha et al. observed the signals of $Al(OP)_4(OH_2)_2$ sites at the chemical shift between −9.5 and −12 ppm.[38] The P_2Al_2 samples synthesized in the presence of surfactant exhibit the ^{27}Al signals with higher intensity than P_1Al_2 samples. However, the reverse case is observed in the samples synthesized in the absence of a surfactant, i.e., higher intensity of the ^{27}Al signals in P_1Al_2 samples, where the spectrum of P_1Al_2-c500 is exceptional. All calcined samples present the tetrahedrally coordinated Al species, which suggests the further cross-linking and condensation of the frameworks during the calcination process, which is in agreement with the structural phase transformation from boehmite to γ-alumina observed by XRD in the calcined products.

The P_1Al_2-d sample synthesized in the presence of a surfactant presents two overlapped ^{31}P NMR peaks, at −6 and −10 ppm, and P_1Al_2-h shows one strong peak at −4.5 ppm, whereas P_1Al_2-c500 gives a spectrum similar to that of P_1Al_2-d but with lower intensity (see Figure 9). The ^{31}P NMR spectra of the surfactant-synthesized P_2Al_2-d and P_2Al_2-c500 are also similar, although the signal intensity of the latter is significantly low. However, the surfactant-synthesized P_2Al_2-h exhibits one peak at −3.5 ppm, with two shoulders at 3 and −11 ppm. Although the surfactantless-

(32) Yuan, Z. Y.; Ren, T. Z.; Azioune, A.; Pireaux, J. J.; Su, B. L. *Catal. Today* **2005**, *105*, 647−654.
(33) Yuan, Z. Y.; Ren, T. Z.; Vantomme, A.; Su, B. L. *Chem. Mater.* **2004**, *16*, 5096−5106.
(34) Muller, D.; Jahn, E.; Ladwig, G.; Haubenreisser, V. *Chem. Phys. Lett.* **1984**, *109*, 332.
(35) Mortlock, R. F.; Bell, A. T.; Radke, C. J. *J. Phys. Chem.* **1993**, *97*, 775−785.
(36) Sayari, A.; Moudrakovski, I.; Reddy, J. S. *Chem. Mater.* **1996**, *8*, 2080−2088.
(37) Moudrakovski, I. L.; Schmachlova, V. P.; Katsarenko, N. S.; Mastikhin, V. M. *J. Phys. Chem. Solids* **1987**, *47*, 335.
(38) Rocha, J.; Kolodziejski, W.; He, H.; Klinowski, J. *J. Am. Chem. Soc.* **1992**, *114*, 4884.

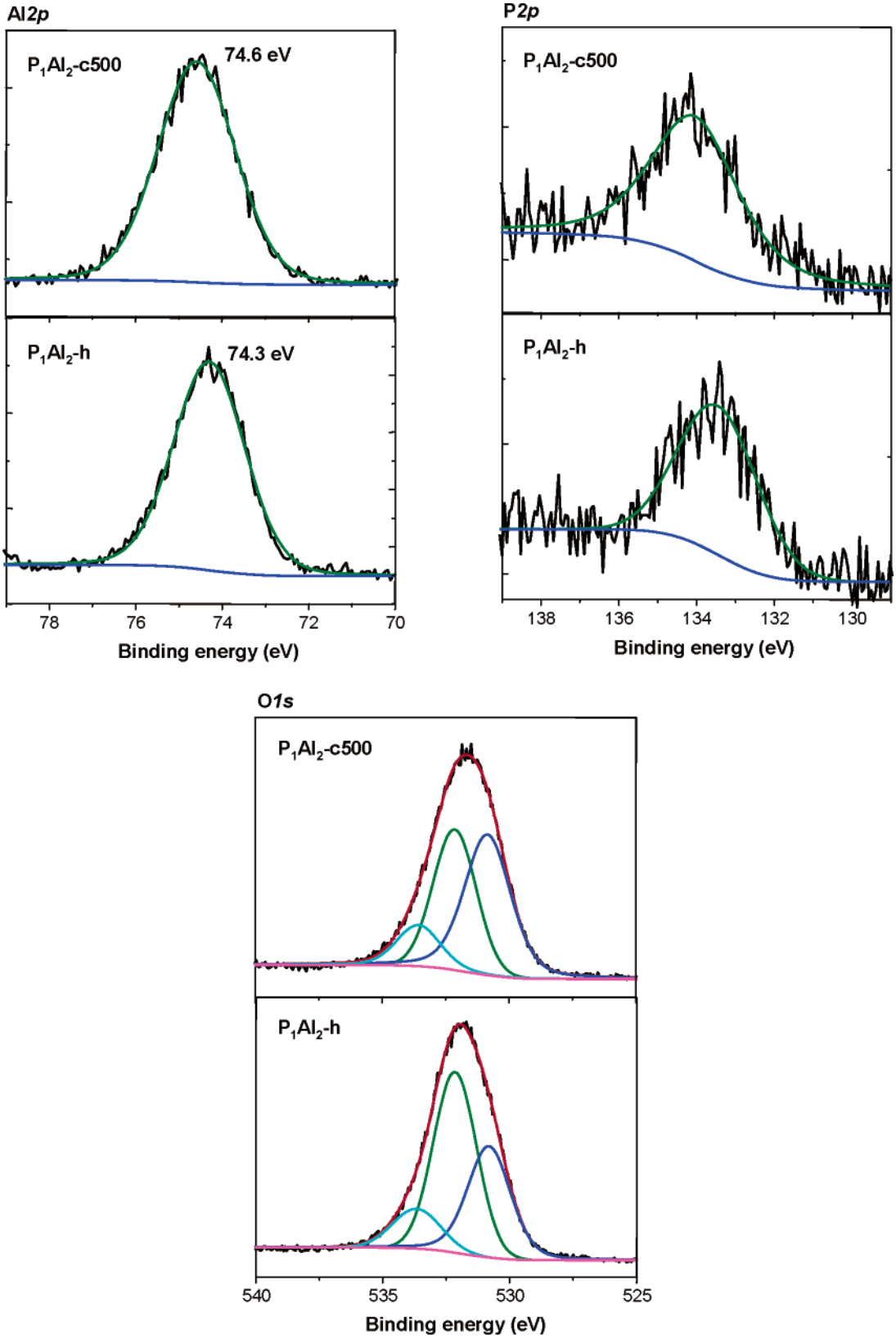

Figure 7. High-resolution X-ray photoelectron spectroscopy (XPS) spectra of the Al 2p, P 2p, and O 1s regions, taken on the surfaces of P_1Al_2-h and P_1Al_2-c500 samples synthesized in the presence of a surfactant.

synthesized P_1Al_2 and P_2Al_2 samples show ^{31}P signals between −4 and −12 ppm that are similar to those of surfactant-synthesized samples, it is interesting that the peak intensity increased after calcination, which is contrary to the case of the surfactant-synthesized samples. It has been reported that the chemical shifts of P atoms change toward high magnetic fields, depending on the number of Al atoms that are bonded to PO_4 units,[39] and the ^{31}P NMR peak at 3 to 5 ppm is assigned to an isolated PO_4 unit (PO_4^{3-}, HPO_4^{2-},

(39) Mortlock, R. F.; Bell, A. T.; Radke, C. J. *J. Phys. Chem.* **1993**, *97*, 767−774.

Table 2. Surface Atomic Compositions Determined by XPS, and ^{27}Al and ^{31}P NMR Chemical Shifts of the Synthesized PAl Samples

	Composition[a] (%)					Chemical Shift (ppm)	
sample	O	Al	P	C	Al/P ratio	^{27}Al[b]	^{31}P
				Synthesized with Surfactant			
P_1Al_2-d	33.70	10.38	1.09	54.84	9.56	7	−6, −10
P_1Al_2-h	50.47	17.76	1.77	30.00	10.05	7, 0, −14	−4.5
P_1Al_2-c500	45.40	18.85	1.77	33.98	10.67	67, (33), 6	−5, −11
P_2Al_2-d	44.50	14.23	1.89	39.39	7.55	6, 0, −14	−7
P_2Al_2-h	50.74	17.46	1.78	30.02	9.79	7	3, −3.5, −11
P_2Al_2-c500	39.04	14.18	1.25	45.53	11.36	67, (33), 6	−6.3
				Synthesized without Surfactant			
P_1Al_2-d	59.98	21.91	1.65	16.46	13.30	67, 35, 6	−7
P_1Al_2-h	49.74	16.63	1.27	32.36	13.06	6	−5, −11
P_1Al_2-c500	33.31	10.77	0.99	54.92	10.85	67, (33), 6	−11
P_2Al_2-d	57.62	20.82	2.53	19.03	8.22	(33), 6, 1, −13.7	−6, −11
P_2Al_2-h	51.59	18.48	1.66	28.27	11.10	7	−4.3
P_2Al_2-c500	44.08	16.98	1.57	37.36	10.81	65, (33), 6, 1, −14	−11.8

[a] Based on XPS line areas of the O 1s, Al 2p, P 2p, and C 1s peaks. [b] The values in parentheses are the chemical shifts of the very weak signals.

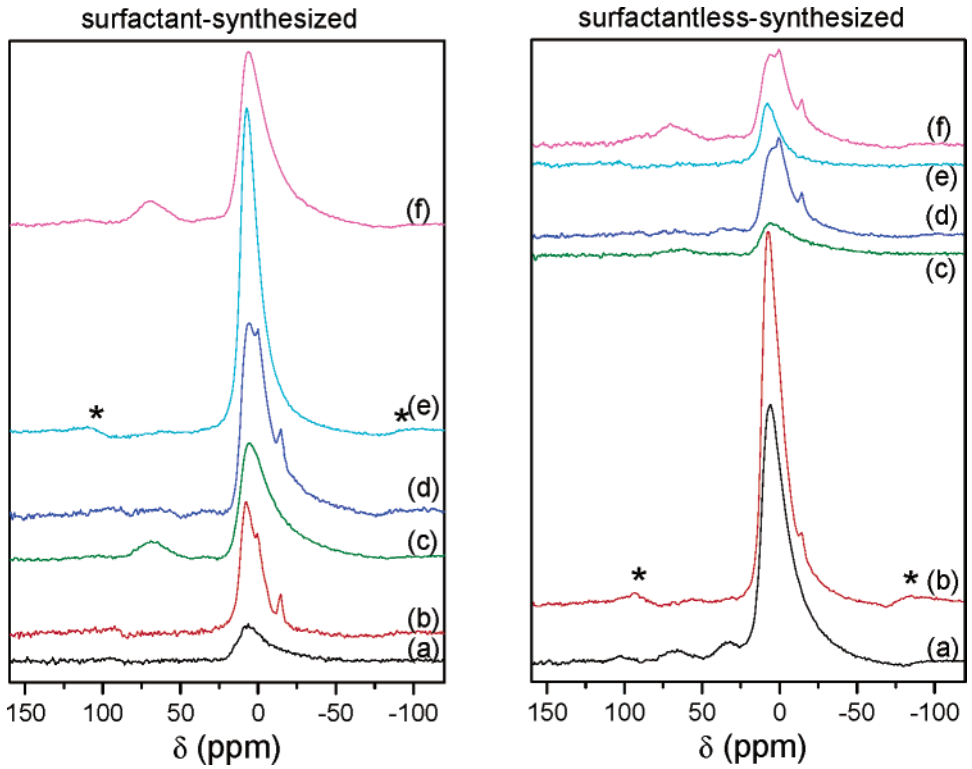

Figure 8. ^{27}Al magic angle spinning nuclear magnetic resonance (MAS NMR) spectra of the PAl samples synthesized in the presence (left) and absence (right) of a surfactant: P_1Al_2-d (spectrum a), P_1Al_2-h (spectrum b), P_1Al_2-c500 (spectrum c), P_2Al_2-d (spectrum d), P_2Al_2-h (spectrum e), and P_2Al_2-c500 (spectrum f). The asterisk symbol (*) indicates spinning sidebands.

$H_2PO_4^-$, or H_3PO_4), the peak at −3.5 to −5.5 ppm is assigned to P nuclei in acid dimers ($H_6P_2O_8$ and $H_5P_2O_7^-$) bonded to one Al atom, the peak at −8.5 to −11 ppm is assigned to $H_2PO_4^-$ ions bonded to one Al atom, the peak at −11 to −13 ppm is assigned to H_3PO_4 molecules bonded to one Al atom, and the peak at −15 to −22 ppm is assigned to P nuclei bridging two Al monomers.[35,39] Thus, the ^{31}P signals at −4 to −7 ppm in our PAl samples can be attributed to polymeric P ligands bonded with one Al atom of the sample surface, e.g., $[Al(H_2O)_5(H_3PO_4)_n]^{m+}$ (where $n \geq 2$ and m is undetermined) or $[Al(H_2O)_4(H_2PO_4)_2]^+$, and the peaks at −11 to −12 ppm are attributed to P nuclei in $[Al(H_2O)_5(H_2PO_4)]^{2+}$ and/or $[Al(H_2O)_5(H_3PO_4)]^{3+}$. The shoulder peak at 3 ppm observed in surfactant-synthesized P_2Al_2-h is attributed to isolated $PO_2(OH)_2$ groups [40] forming the surface layers of the surfactant-phosphoric acid complex,[36] which disappeared in the calcined product. Compared with the spectra of PAl-h samples and their calcined products PAl-c500, the ^{31}P peaks shift toward higher magnetic field after calcination, indicating that the calcination process promotes the further condensation of the frameworks.

Fourier Transform Infrared Spectroscopy. The FT-IR spectra of the KBr-supported phosphated samples of P_1Al_2-h and P_1Al_2-c500 synthesized in the presence and absence of a surfactant are shown in Figure 10. The spectra of the surfactant-synthesized samples are similar to the surfactant-less-synthesized samples. The absorption bands at 3430 and 1630 cm^{-1}, possessed by all the samples, correspond to the specificity of water molecules adsorbed on OH groups and bending vibrations of these surface-adsorbed water mol-

(40) Hartman, P.; Vogel, J.; Schnabel, B. *J. Magn. Reson.* **1994**, *111*, 110.

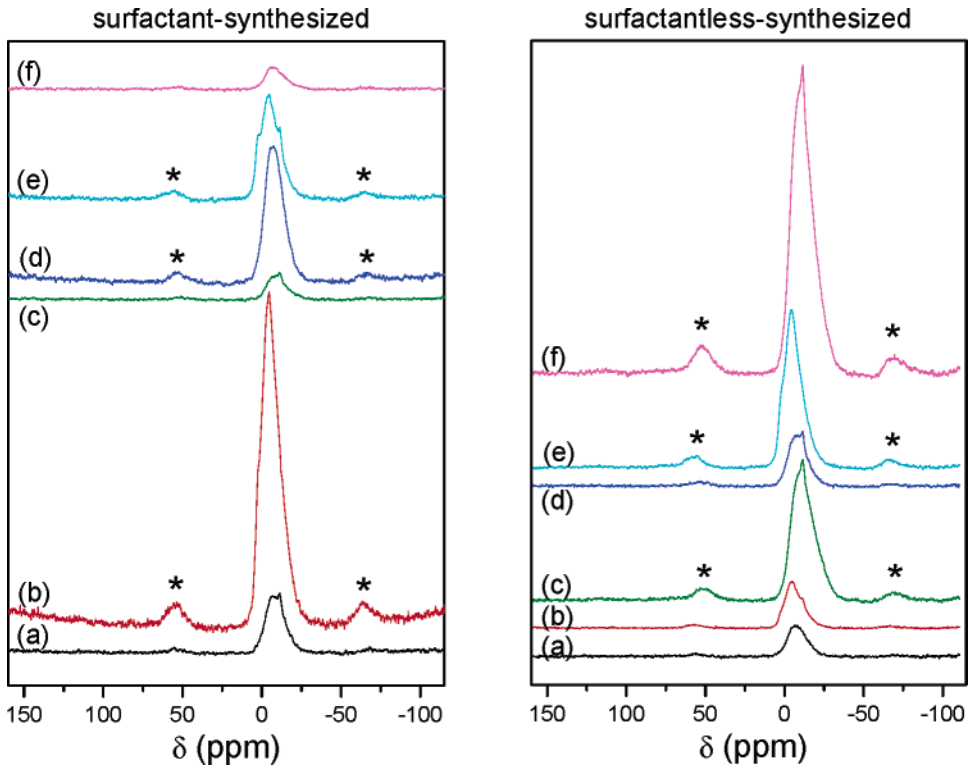

Figure 9. ^{31}P MAS NMR spectra of the PAl samples synthesized in the presence (left) and absence (right) of a surfactant: P_1Al_2-d (spectrum a), P_1Al_2-h (spectrum b), P_1Al_2-c500 (spectrum c), P_2Al_2-d (spectrum d), P_2Al_2-h (spectrum e), and P_2Al_2-c500 (spectrum f). The asterisk symbol (*) indicates spinning sidebands.

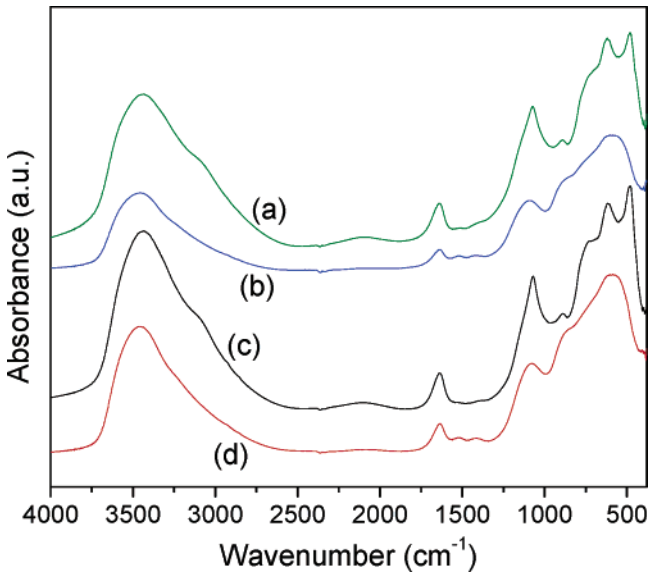

Figure 10. Fourier transform infrared (FT-IR) spectra of P_1Al_2-h and P_1Al_2-c500 synthesized in the absence of surfactant (spectra a and b, respectively), and P_1Al_2-h and P_1Al_2-c500 synthesized in the presence of a surfactant (spectra c and d, respectively).

ecules, respectively.[41] The weak shoulder bands at ∼3110 cm^{-1} in the spectra of the P_1Al_2-h samples could be attributed to the organic species adsorbed in the samples, which disappeared after calcination at 500 °C. The bands at 1110−1070 cm^{-1} are due to P−O bond vibrations,[42] which broadened in the calcined samples. The P_1Al_2-h samples also present two strong adsorption bands, at 620 and 490 cm^{-1}, as well as a small band at 890 cm^{-1} and a shoulder band at ∼730 cm^{-1}. The bands at 620 and 490 cm^{-1} are assigned to the Al−O vibrations of boehmite AlOOH,[43,44] which transformed to one unsplit and broad band centered at 590 cm^{-1}, which is characteristic of pure γ-Al_2O_3, after a calcination of the samples. The small band at 890 cm^{-1} may be due to the Al−O−Al and/or Al−O−P vibrations, which intensity increased in the calcined samples. The shoulder bands at ∼730 cm^{-1}, which correspond to P−O−P deformation vibrations,[45] are not observed in the IR spectra of calcined samples.

To get insight into the surface structure and acidity of the synthesized PAl samples, the FI−IR spectra in vacuo of the materials were taken at room temperature after outgassing at the temperature of 400 °C over 3 h, following the adsorption of ammonia molecules at room temperature and desorption at various temperatures from 100 °C to 300 °C; these are shown in Figure 11 (a series of surfactant-synthesized P_1Al_2 samples are only taken as being representative). The spectrum of the outgassed P_1Al_2 sample possesses one absorption band at 3670 cm^{-1} with a shoulder at 3735 cm^{-1}, which has been assigned to the surface P−OH and Al−OH groups respectively,[46] superimposed on one broad band at ∼3580 cm^{-1} corresponding to hydrogen-

(41) Ren, T.-Z.; Yuan, Z.-Y.; Su, B.-L. *Chem. Phys. Lett.* **2003**, *374*, 170−175.
(42) Steger, E.; Schmidt, W. *Ber. Bunsen−Ges. Phys. Chem.* **1964**, *68*, 102.
(43) Music, S.; Dragcevic, D.; Popovic, S. *Mater. Lett.* **1999**, *40*, 269−274.
(44) Geiculescu, A. C.; Strange, T. F. *Thin Solid Films* **2003**, *426*, 160−171.
(45) Busca, G.; Lorenzelli, V.; Galli, P.; Ginestra, A. L.; Patrono, P. *J. Chem. Soc., Faraday Trans. 1* **1987**, *83*, 853.
(46) Peri, J. B. *Discuss Faraday Soc.* **1971**, *52*, 55−65.

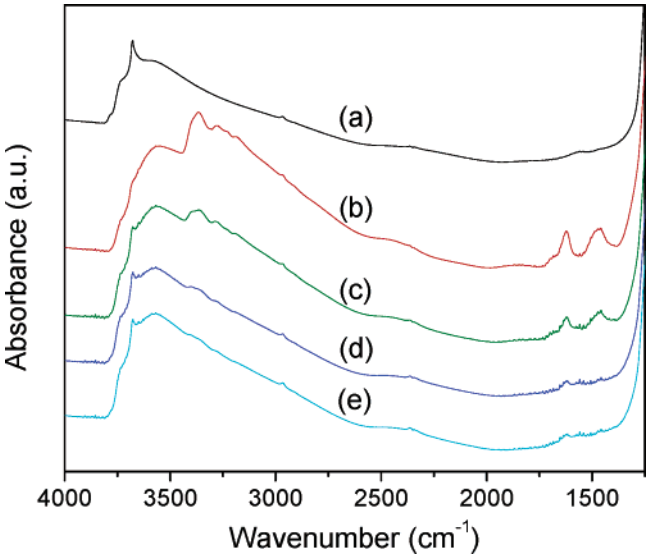

Figure 11. In situ FT-IR spectra of the surfactant-synthesized P_1Al_2-h samples: after evacuation at 400 °C for 3 h (spectrum a), and then after adsorption of NH_3 at room temperature for 15 min (spectrum b), desorption at 100 °C for 15 min (spectrum c), desorption at 150 °C for 15 min (spectrum d), and desorption at 200 °C for 15 min (spectrum e).

bonded (associated) hydroxyl groups.[47] The presence of the P−OH groups is normally indicative of the weak Brönsted acid sites.[32] After in situ adsorption of NH_3, the bands of the Al−OH and P−OH groups almost disappear, and one new band at 3361 cm^{-1} and a shoulder at ∼3270 cm^{-1}, stemming from the interaction of NH_3 with Al−OH and P−OH groups at 3735 and 3670 cm^{-1}, respectively, that can be shifted toward lower wavenumbers,[48] and two new bands (at ∼1620 and 1465 cm^{-1}, corresponding to the surface adsorbed NH_4^+ groups), appear (see Figure 11b). Thus, it is believed that the NH_3 molecules are indeed absorbed on the acid sites where Al−OH and P−OH groups are presented. The following desorption at 100 °C led to the emergence of the bands of 3735 and 3670 cm^{-1} again, and the weakening of the bands at 3400−3260 cm^{-1} and 1650−1450 cm^{-1}. Further desorption at the elevated temperatures conducted to the recovery of the intensity of the bands of Al−OH and P−OH groups, and the decrease, even disappearance in intensity of the bands of NH_4^+ groups (see Figure 11e), indicating that the ammonia adsorption and desorption processes are reversible.

Thermal Analysis. Thermogravimetric analysis of the as-synthesized PAl samples was performed to understand the thermal properties of the obtained materials. Figure 12 presents the thermogravimetry−differential scanning calorimetry (TG−DSC) profiles of the surfactant-synthesized P_2Al_2-d and surfactantless-synthesized P_1Al_2-h, showing a continuous weight loss of 47.6 and 26.5 wt % from room temperature to 600 °C, respectively. Taking into account the combination of differential thermogravimetry (DTG), four weight losses of surfactant-synthesized P_2Al_2-d can be observed: the first two weight losses (I and II) of ∼19.5% below ∼200 °C, which may be assigned to the desorption of water (that may be physical or chemical adsorption on the interparticle surface of the sample or reside the channels) and the desorption and even partial decomposition of the adsorbed organic species originated from the alkoxide hydrolysis, and the third weight loss (III), which is superimposed with a fourth weight loss (IV), with a total weight loss of 27.1%, between 200 and 500 °C, attributed to the decomposition of the surfactant, and to the dehydration of AlOOH to Al_2O_3,[27,49,50] respectively. However, only two evident weight losses of the surfactantless-synthesized P_1Al_2-h can be detected: the weight loss (I) of ca. 14% below 200 °C, which is due to the desorption of water, and the weight loss (IV) of 11.0% between 200 and 500 °C, which is due to the structural transformation of AlOOH to Al_2O_3. This is in agreement with the XRD observation that a 500 °C calcination can completely convert AlOOH to γ-Al_2O_3. It also suggests that the surfactant molecules can be completely removed at the calcination temperature (500 °C) used in this work, and the synthesized PAls are thermally stable.

Storageability. It is known that zeolite-like molecular sieves and mesoporous materials are mostly metastable, and difficult to be stored for a long time. Thus, it may be significant to further investigate the storageability of the present mesoporous−macroporous PAl materials. After 16 months of storage, the PAl samples still exhibited isotherms that were similar to the freshly synthesized samples (see the Supporting Information), although their porosities and textural properties have degenerated (Table 3). The surfactant-synthesized PAl-d samples show two overlapped peaks, at 3.6 and 6.8 nm, in their pore size distribution curves, with the lower surface areas and pore volumes than the fresh-synthesized PAl-d. The surfactant-synthesized PAl-h samples are still bimodal, but with the enlarged pore sizes (3.2−3.5 nm and 19.5−23.2 nm) and reduced surface areas and pore volumes (∼420 m^2/g and ∼2.3 cm^3/g, respectively), which are comparable with the freshly synthesized pure aluminum oxides yet. The surfactantless-synthesized PAl samples also exhibited the reduced surface areas and pore volumes and the enlarged pore sizes after 16 months of storage (see Table 3). This observation indicates that the long-term storage would damage the mesoporous structures of the PAl samples, in a manner similar to the case of most as-synthesized mesoporous materials. However, the well-defined macroporous structures can be observed significantly in these 16-month-stored PAl samples.

Discussion. A panoramic examination of the synthesized PAl samples via SEM has revealed a larger quantity of macroporous particles in the surfactant-synthesized samples than in the surfactantless-synthesized samples, and more particles of macroporous structures in the autoclaved samples than in the nonautoclaved ones. This observation is indeed supported by the nitrogen adsorption analysis. It is well-known that the macroporosity can be certainly reflected on the N_2 adsorption isotherms at the high P/P_0 range, although the most direct evidence may be from the mercury extrusion

(47) Ballinger, T. H.; Yetes, T., Jr. *Langmuir* **1991**, *7*, 3041.
(48) Su, B. L.; Barthomeuf, D. *J. Catal.* **1993**, *139*, 81−92.
(49) Wells, A. F. *Structural Inorganic Chemistry*, 4th Edition; Clarendon Press: Oxford, U.K., 1975.
(50) Lee, J. D. *Concise Inorganic Chemistry*, 5th Edition; Blackwell Science: Oxford, U.K., 1998.

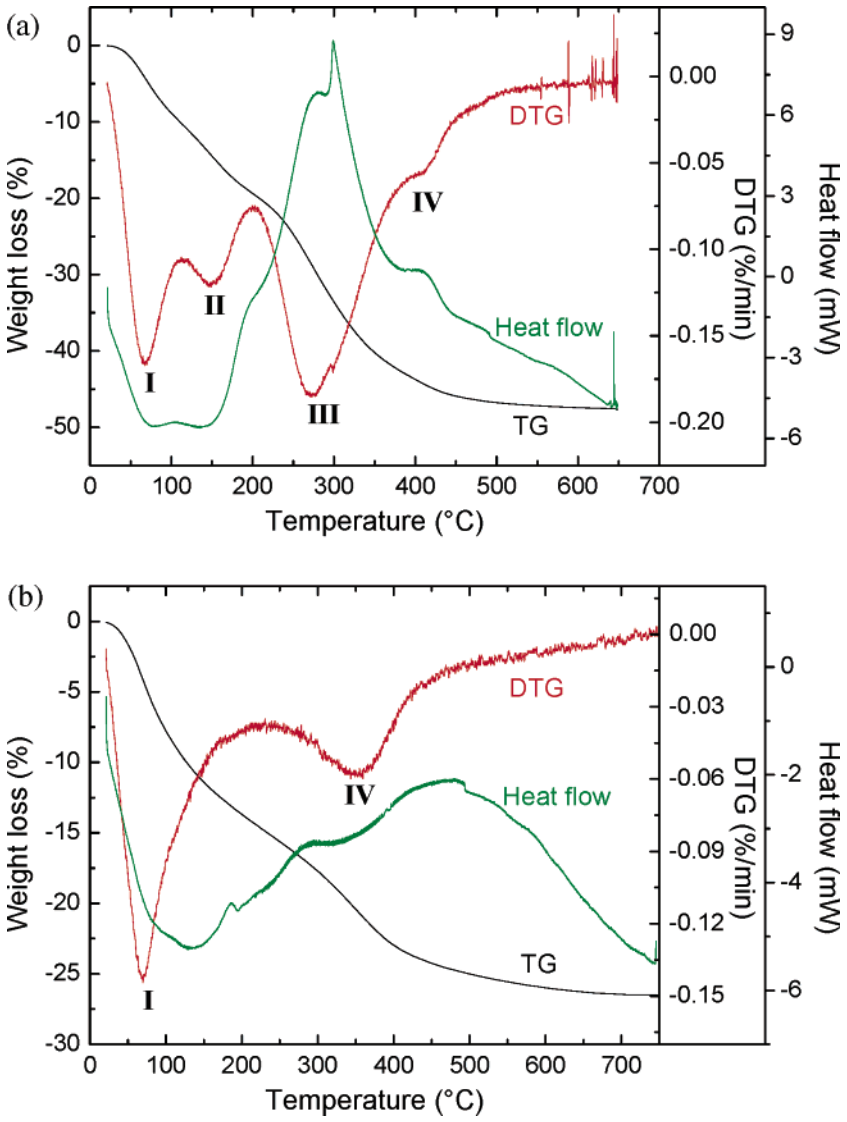

Figure 12. Thermogravimetry−differential scanning calorimetry (TG−DSC) profiles of (a) the surfactant-synthesized P_2Al_2-d sample and (b) the surfactantless-synthesized P_1Al_2-h sample.

Table 3. Textural Properties of the PAl Samples after 16 Months of Storage

sample	BET surface area, S_{BET} (m^2/g)	nitrogen pore volume, V_{pore}[a] (cm^3/g)	$D_{BJH-ads}$[b] (nm)	Average Pore Diameter, from BJH Analysis (nm)	
				absorption, D_{av-ads}[c]	desorption, D_{av-des}[c]
Synthesized without Surfactant					
P_1Al_2-d	130	0.29	7.6	6.8	5.6
P_1Al_2-h	263	0.41	3.4	5.1	4.4
P_2Al_2-d	131	0.32	8.2	7.7	6.1
P_2Al_2-h	262	0.36	3.6	4.6	3.9
Synthesized with Surfactant					
P_1Al_2-d	107	0.28	3.6, 6.8	7.0	5.4
P_1Al_2-h	415	2.31	3.5, 19.5	18.5	16.1
P_2Al_2-d	138	0.36	3.6, 6.8	7.1	5.8
P_2Al_2-h	427	2.28	3.2, 23.2	17.8	15.2

[a] At $P/P_0 = 0.993$. [b] Maximum of BJH pore diameter distribution as determined from the adsorption branch. [c] BJH average pore diameter (4V/A).

technology and/or electron microscopy. The strong uptake in N_2 adsorbed volume at $P/P_0 > 0.85$ is the result of macroporosity. Such an uptake is quite strong in the isotherms of the surfactant-synthesized PAl-h and their calcined products, in comparison with the PAl-d prepared in the presence of surfactant, and the PAl samples synthesized in the absence of a surfactant, indicating the very large macroporosity in the surfactant-synthesized autoclaved PAl samples. In addition, the macroporosity of the surfactant-synthesized PAl-h is even larger than the reported mesoporous−macroporous pure aluminum oxides, as revealed by the comparison of the isotherms with the surfactant-synthesized autoclaved pure aluminum oxides.[16]

Furthermore, the direct phosphation and autoclaving take significant roles in not only the macroporosity but also the textural properties of the resultant PAl samples. In compari-

son with the specific surface areas of PAl-h and PAl-d, it is observed that the surface areas of PAl-h are higher than that of PAl-d, regardless of whether it was synthesized with or without a surfactant. The surface areas of the surfactant-synthesized PAl-h and their calcined products are also higher than those of pure aluminum oxide materials synthesized under similar conditions but without phosphates.[16] The mesopore sizes and surface areas of the PAl-d samples synthesized with surfactant are lower than those prepared without a surfactant. This may be due to the existence of a small quantity of organic surfactant species in the pore channels of the surfactant-synthesized PAl-d samples, which was evidenced by the TG analysis (see Figure 12). However, the surfactant-synthesized PAl-h samples exhibit very high surface areas and large pore volumes (>730 m^2/g and >3.4 cm^3/g, respectively) with bimodal mesopore size distributions ($\sim$3 nm and 16.8−19.4 nm), distinct from the surfactantless-synthesized PAl-h (which exhibits a surface area of 377 m^2/g and unimodal mesopores 2.4−2.7 nm in size), as well as pure AlOOH synthesized with surfactant (which has a surface area of 381 m^2/g and mesopore size of 3.0 nm).[16] Such hierarchical trimodal mesoporous−macroporous PAl materials should be of great interest, from the technological point of view, although the 3-nm-sized mesopore structure of surfactant-synthesized PAl-h would be more or less damaged after calcination at 500 °C or above. After calcination at elevated temperatures, the surface areas decrease as the calcination temperature increases, while the mesopore sizes increase, regardless of whether the PAl-h samples were synthesized with or without a surfactant. This trend is similar to the case of mesoporous materials that have been obtained via a nanoparticle assembly mechanism.[3,4,41,51] It is remarkable that the exceedingly high surface areas of 360−392 m^2/g and large pore volumes of 2.37−2.60 cm^3/g can still be obtained after calcination of the surfactant-synthesized PAl samples at 800 °C, which is quite attractive, considering their application potential. Moreover, in regard to the surfactantless-synthesized PAl samples, the calcination of PAl-h at 500 and 800 °C led to the pore size enlargement of only 1−1.2 nm and 5.5−6.6 nm, respectively. A mesopore size enlargement of 5.8 and 9.2 nm was observed for the surfactant-synthesized pure aluminum oxide after calcination at 500 and 800 °C, respectively. However, the step of mesopore size enlargement of the surfactant-synthesized PAl samples is also substantially small. Thus, it is evident that the direct phosphation resulted in the considerable improvement of the thermal stability, and the surfactant contributed to the improvement of the surface areas and porosities during the PAl formation.

Because macroporous structures could be found in the PAl-d samples, even in the surfactant-free synthesis, the formation of the macroporous structures with nanostructured walls is considered to be spontaneous. No templates or structure-directing agents are necessary for the creation of a hierarchical mesoporous−macroporous structure. The pre-proposed mechanism of a surfactant supermicelle-induced macrostructure formation[16,21] is not applicable in this work anymore. The hydrolysis of aluminum alkoxide precursors in the acidic solution would result in the rapid formation of nanometer-sized AlOOH particles via the reaction of $Al(OR)_3 + 2H_2O \rightarrow AlOOH + 3ROH$. Because the presence of H_3PO_4 and HPO_4^{2-} in the solution should lead to the formation of a buffer solution, which may drive the gentle formation of phosphated AlOOH nanoparticles with good size and homogeneity and promote the regular assembly of the nanoparticle, a network of narrow mesoporous channels could be created in the aggregation of the nanoparticles. Meanwhile, many butanol molecules were generated quickly by the hydrolysis of aluminum *sec*-butoxide in phosphatic solution and polycondensation, which might produce microphase-separated domains of PAl-based nanoparticles and water/alcohol channels that are the initiators and the driving force for the formation of the macrochannels.[24,52] Thus, a hierarchical structure of uniform macrochannels with mesoporous walls of nanoparticle assembly would form during the synergistic packing of the nanoparticles and rapid release of alkanol molecules. Autoclaving would consolidate the regular self-assembly of the nanoparticles to create a well-connected network of mesoporous−microporous walls between macrochannels and, meanwhile, contribute to the phase transformation from amorphous/noncrystalline to crystalline (boehmite), which is evident by the XRD patterns.

N_2 adsorption analysis and TEM images also demonstrated that uniform mesoporous structures could be obtained even in the absence of a surfactant, although previous work with the mesostructured alumina synthesis accentuated the role of the surfactant in the nanoparticle assembly process of mesostructures.[2−4] Thus, the surfactant did not seem to have any directing role in the generation of both macroporous and mesoporous structures. However, the surfactant-synthesized PAl samples have higher surface areas and larger pore volumes than the surfactantless-synthesized samples, as well as the distinct mesoporous size distributions. In addition, greater macroporosity is observed in the surfactant-synthesized samples. This suggests that the surfactant molecules may affect the precipitation and aggregation of the phosphated AlOOH nanoparticles, leading to an indirect influence on the generation of a hierarchical mesoporous−macroporous structure.

Note that the initial pH values of the mixed solution of H_3PO_4 and Na_2HPO_4 in the P_1Al_2 and P_2Al_2 synthesis system were 2 and 3, respectively, which almost did not change in the synthesis process with a surfactant during the hydrolysis of aluminum *sec*-butoxide; however, these pH values changed to $\sim$6 in the surfactant-free synthesis process. Thus, the difference in the textural properties of the surfactant-synthesized and surfactantless-synthesized PAl samples should be related to this pH change, although we do still not totally understand the reason the pH system of buffer solution could be preserved when in the presence of surfactant molecules.

Although the initial gel involved different P/Al ratios for the synthesis of P_1Al_2 and P_2Al_2, the surface atomic

(51) Yuan, Z. Y.; Ren, T. Z.; Su, B. L. *Catal. Today* **2004**, *93*−*95*, 743−750.

(52) Ren, T. Z.; Yuan Z. Y.; Su, B. L. *Chem. Phys. Lett.* **2004**, *388*, 46−49.

compositions of the obtained samples are similar (Al/P ratios of 8−13), as revealed by XPS data. This indicates that the quantity of phosphorus in the phosphation is inflexible. Most of the detected P atoms may be on the surface of aluminum (oxyhydr)oxide particles, but mainly link with Al via O in the form of P−O−Al, which is further confirmed by FT-IR and solid-state NMR spectroscopy. Such a formed thin layer of aluminum phosphate should be amorphous, even after calcination at high temperature, because no detectable $AlPO_4$ phase was observed in the XRD patterns.

The IR peaks at 1100−1250 cm^{-1} are often the characteristic frequencies of PO_4^{3-}, and the broadening of this band is the result of reducing the symmetry in the free PO_4^{3-} (Td point group). Although one peak, at ∼1100 cm^{-1}, was observed in our PAl samples, the absence of the phosphoryl (P═O) band at 1300−1400 cm^{-1} does not support the presence of PO_4^{3-} ions in the particle surface. Thus, we believe that the phosphorus exists as Al−O−P in the obtained PAl samples.[12] Most of the phosphorus is in the form of H_2PO_4 bonded with one Al atom through O atoms, besides a small quantity of polymeric phophorus ligands (i.e., acid dimers) due to the presence of a weak band of P−O−P deformation vibration at the ∼730 cm^{-1} bond. This is consistent with the ^{27}Al and ^{31}P NMR results. Most of the Al atoms exist in an octahedral coordination, and the four-coordinated Al can be seen in the calcined samples.

Calcination at elevated temperature could lead to the topochemical transformation from aluminum oxyhydroxide boehmite to γ-Al_2O_3. However, as revealed by XRD, N_2 adsorption, and electron microscopy, the direct phosphation has improved the thermal stability, as a result of the inhibition of grain growth of the embedded alumina by the interspersed amorphous aluminum phosphate matrix during thermal treatment. The mesoporous−macroporous structure with a high surface area and porosity can be retained during the transformation process from boehmite to γ-alumina upon calcination at 800 °C.

FT-IR spectra also revealed the existence of a large quantity of surface hydroxyl groups, including Al−OH and P−OH, even after evacuation at 400 °C. The spectra of NH_3 adsorption did indicate the presence of the Brönsted acid sites in these hierarchical PAl samples, although they are weaker than zeolitic hydroxyls.[48,53,54] The large number of surface hydroxyl groups is really significant to be used as active sites in catalysis or binding sites for surface modification in the multifunctionalization of the sample surface, to extend the possible applications to advanced functional materials.[41] In the calcined PAl samples, a significant quantity of tetrahedral-coordinated Al was observed, which can act as Lewis acid sites. These Lewis acid sites can easily adsorb oxygen and water molecules.

The hierarchical porous materials are indeed of great significance, because of their important role in the systematic study of structure−property relationships and their technological promise in applications.[14] Our synthesized phosphated aluminum (oxyhydr)oxide materials are crystalline or semicrystalline with high surface areas and thermal stability, possessing not only the hierarchical macroporous structures with mesoporous walls but also a large number of surface hydroxyl groups and acid sites. Such a hierarchical porous structure enables our synthesized PAl samples to efficiently reduce diffusion resistance of molecules for yielding improved overall reaction, which are really desirable catalysts or catalyst supports for the design of structured catalysts, or one-pot reactors. This work has demonstrated the self-assembly of hierarchically mesoporous−macroporous nanocrystalline PAl-based materials with a uniform macropore array and narrow mesopore size distribution, without the use of polymer latex spheres, as usually reported for the creation of macropores. The direct incorporation of phosphorus has enabled the stabilization of the mesoporous−macroporous structure of aluminum oxides, offering a homogeneous distribution of phosphorus in the form of surface P−O−Al bonding. This method can be applicable for the preparation of various hierarchical composite materials with multiscaled porosity.

Conclusions

Hierarchically mesoporous−macroporous phosphated aluminum (oxyhydr)oxide materials with very high surface areas and thermal stability have been prepared. The macroporous framework is (semi)crystalline with accessible mesopores of a scaffold-like nanoparticle assembly. The use of surfactant was determined to influence the textural properties and porosity of the resultant PAl materials, but not to direct the formation of macroporous structures. The direct phosphation in the H_3PO_4 and HPO_4^{2-} solution of the synthesis system led to the incorporation of phosphorus into the framework of the mesoporous−macroporous structure of aluminum (oxyhydr)oxides, improving their thermal stability. The grain growth is inhibited and the surface area is increased significantly, because a thin layer of amorphous aluminum phosphate was formed, which is attached on the surface of the (semi)crystalline alumina nanoparticles. Moreover, these synthesized mesoporous−macroporous PAl samples possess acid sites and surface hydroxyl groups, which are believed to be significant and find practical application potential in the fields of catalysis and materials science.

Acknowledgment. This work was supported by the European Program of InterReg III (Program France-Wallonie-Flandre, FW-2.1.5), the Belgian Federal Government (PAI-IUAP 01/5 project), the National Natural Science Foundation of China (No. 20473041), and the National Basic Research Program of China (No. 2003CB615801).

Supporting Information Available: N_2 adsorption analysis of the mesoporous−macroporous phosphated aluminum (oxyhydr)-oxide materials (PDF). This material is available free of charge via the Internet at http://pubs.acs.org.

CM0520160

(53) Su, B. L.; Norberg, V. *Zeolites* **1997**, *19*, 65−74.
(54) Jaumain, D.; Su, B. L. *Catal. Today* **2002**, *73*, 187−196.